

# Oxide interfaces: pathways to novel phenomena

Novel phenomena and functionalities at artificial heterointerfaces have been attracting extensive scientific attention in both materials science and fundamental condensed matter physics. The interplay between degrees of freedom at interfaces of complex oxides could lead to exotic and unexpected states of matter. In this article, using the model system of  $\text{BiFeO}_3$  and  $\text{La}_{0.7}\text{Sr}_{0.3}\text{MnO}_3$ , we review recent progress on our understanding of the novel states formed at this heterointerface. Furthermore, we discuss how emergent interfacial phenomena can be employed to influence the bulk properties of these materials. We summarize by highlighting several possible and promising directions for future study.

Pu Yu<sup>1,2\*</sup>, Ying-Hao Chu<sup>1,3,4</sup> and Ramamoorthy Ramesh<sup>1,3</sup>

<sup>1</sup> Department of Physics and Department of Materials Science and Engineering, University of California, Berkeley, CA 94720, USA

<sup>2</sup> State Key Laboratory for Low-Dimensional Quantum Physics, Department of Physics, Tsinghua University, Beijing 100084, the People's Republic of China

<sup>3</sup> Materials Science Division, Lawrence Berkeley National Laboratory, Berkeley, CA 94720, USA

<sup>4</sup> Department of Materials Science and Engineering, National Chiao Tung University, Hsinchu, Taiwan 30010

\*Email: [yupu.phy@gmail.com](mailto:yupu.phy@gmail.com)

In strongly correlated complex oxides, charge, spin, orbital, and lattice degrees of freedom co-exist and interplay cooperatively, and the correlation between these degrees of freedom and related couplings generate a rich spectrum of competing phases and physical responses, including high temperature superconductivity<sup>1</sup>, metal-insulator transitions<sup>2</sup>, colossal magnetoresistance<sup>3-5</sup>, (anti-) ferromagnetism, (anti-) ferroelectricity<sup>6</sup>, piezoelectricity, and more recently multiferroic<sup>7-9</sup> properties. This has led to extensive studies of both bulks and thin films, with the aim of increasing our understanding of the fundamental nature of existing materials systems, so that we might be able to better control and design novel materials for applications.

In light of the rapid development of state-of-the-art deposition tools, such as oxide molecular beam epitaxy, reflection high-energy electron diffraction (RHEED)-assisted pulsed laser deposition (PLD), sputtering

deposition, and atomic layer deposition, it is now practical to routinely fabricate atomically perfect heterostructures of complex perovskites (Fig. 1a). Fascinating phenomena and novel states of matter at complex oxide heterointerfaces have been reported<sup>10-19</sup>, and are continually expanding the horizon of our knowledge, suggesting that complex oxides are promising candidates for a new generation of electronics<sup>20-24</sup>.

Motivated by this, current research is primarily focused on probing and understanding the novel interfacial phenomena in complex-oxide heterostructures. Although new techniques have allowed us to delve deeper into materials at increasingly smaller length scales, it is also possible to use interfacial structures to control the *bulk* state of an epitaxial layer away from the interface. Such an approach can be realized if one of the layers has long-range spontaneous ordering, such as ferroelectricity or ferromagnetism. For non-ferroic systems, the correlation between two layers is highly confined to a region close to the interface. Far away from

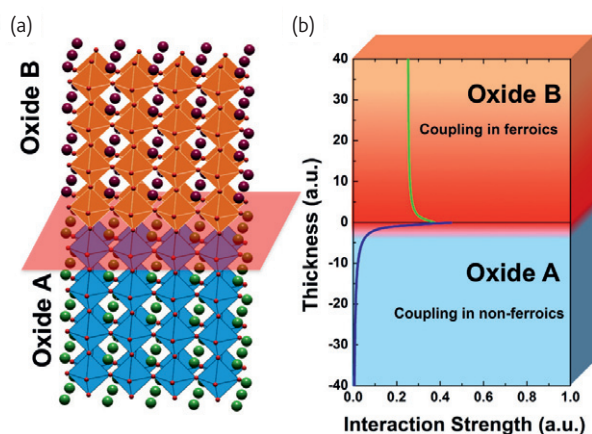


Fig. 1 Schematic of interfacial control of bulk properties. (a) Schematic of a heterostructure built with two perovskites stacked along the [001] direction. (b) Schematic of interface coupling strength through heterointerfaces. In regular materials, the influence of interface coupling is mainly limited to the interface. While for the materials with long-range spontaneous orders, the interface coupling can propagate all the way through the bulk material, providing a novel pathway for the control of bulk properties through interface engineering.

the interface, the effect will be screened and dramatically suppressed. However, this effect can be totally different when one of the layers is ferroic (ferromagnetic or ferroelectric) in nature. The long-range spin or charge order will assist the interface coupling to propagate through the whole layer; thus the interface coupling has a more significant influence to the whole bulk (Fig. 1b). In this regard, the heterostructure of multiferroic (ferroelectric and antiferromagnetic) BiFeO<sub>3</sub> (BFO) and ferromagnetic La<sub>0.7</sub>Sr<sub>0.3</sub>MnO<sub>3</sub> (LSMO) provides us with an excellent platform for such studies. In both materials, the charge, spin, orbital, and lattice degrees of freedom are all fundamentally important in determining the intrinsic properties<sup>3-5,25,26</sup>; thus the interplay between these degrees of freedom across the interface provides an ideal model, allowing us to explore and understand the rich physics involved at heterointerfaces (Fig. 2). Moreover, such interfacial phenomena can be further employed to influence the bulk properties through the ferroelectric (ferromagnetic) nature of the BFO (LSMO) layer<sup>27-29</sup>. In this review, we begin with a discussion of epitaxial design of BFO/LSMO heterointerfaces. Then we turn the focus to the interplay and reconstruction between the various degrees of freedom and the effects they have on the bulk properties. Finally, we highlight some possible and promising directions for future study.

### Epitaxial design of heterointerfaces

Since both BFO and LSMO have the ABO<sub>3</sub> perovskite structure, two possible atomic stacking sequences can be formed in [001]-oriented heterostructures, namely La<sub>0.7</sub>Sr<sub>0.3</sub>O-(MnO<sub>2</sub>)-BiO-FeO<sub>2</sub> (MnO<sub>2</sub>-terminated interface) and MnO<sub>2</sub>-(La<sub>0.7</sub>Sr<sub>0.3</sub>O)-FeO<sub>2</sub>-BiO (La<sub>0.7</sub>Sr<sub>0.3</sub>O-terminated interface). In order to realize this interfacial design, atomically precise interface control is needed and can be achieved by designing LSMO layers with well defined atomic terminations using RHEED controlled PLD growth. During the growth of LSMO layers, a clear intensity oscillation of the specular reflection spot (Fig. 3a) indicates a layer-by-layer growth mode with unit cell precision. Thus, starting with

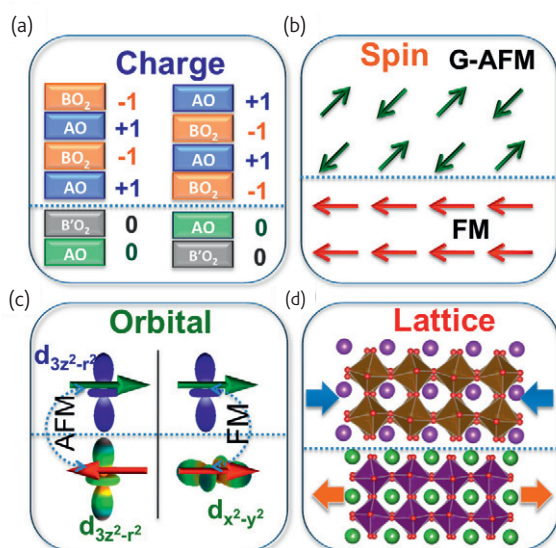


Fig. 2 Illustrations of interplays between degrees of freedom across heterointerfaces. (a) Charge reconstruction across the interface due to polar discontinuity (valence mismatch). (b) Spin reconstruction across the interface due to spin frustration. (c) Correlations between interface orbital occupations and magnetic couplings. (d) Lattice reconstruction due to the mismatch between the lattice constants and oxygen octahedral rotations across the interface.

chemically treated, TiO<sub>2</sub>-terminated STO (001) substrates<sup>30</sup>, LSMO is MnO<sub>2</sub>-terminated. If one desires a change in the surface termination to La<sub>0.7</sub>Sr<sub>0.3</sub>O, the intrinsic surface termination of the STO substrate has to be modified. One possible approach to solve this is to use the inherent difference in surface desorption dynamics of Sr and Ru in SrRuO<sub>3</sub> (SRO)<sup>31</sup>. If a thin layer of SRO (e.g., three unit cells) is deposited onto the TiO<sub>2</sub> terminated STO substrate, the surface is ostensibly terminated as a RuO<sub>2</sub> layer. However, if this layer is maintained at its growth temperature for a short period, the Ru is desorbed from the surface, thus effectively converting it to a SrO-terminated surface. How does one ascertain that this has happened? Surface chemical spectroscopy can help in this regard and this is described briefly, below.

For both films, the topography of both samples (Fig. 3b) shows the presence of atomically flat terraces as defined by the underlying vicinal substrate and separated by steps of height ~ 0.4 nm (~ one perovskite unit cell). Thus, the films grown in such a manner must be singly terminated. To further confirm the surface compositions of LSMO thin films with different terminations, time-of-flight ion scattering and recoiled ion spectroscopy (TOF-ISARS) were used (Fig. 3c); which are capable of highly sensitive surface analysis with isotopic resolution<sup>32</sup>. The results (Fig. 3d) reveal that the LSMO films grown on the SRO buffer layers exhibit strongly enhanced La- and Sr-peak intensities as compared to the samples grown directly on a TiO<sub>2</sub> terminated STO, which suggests that the surface composition of the film is indeed La- and Sr-rich. Combining this with the topography data, it is possible to ascertain that the terminations of the LSMO layers can be controlled by the growth with atomic precision. While the studies so far have shown the qualitative efficacy of the SRO buffer layer approach, much needs to be understood regarding quantification of the TOF-ISARS data. This would enable one

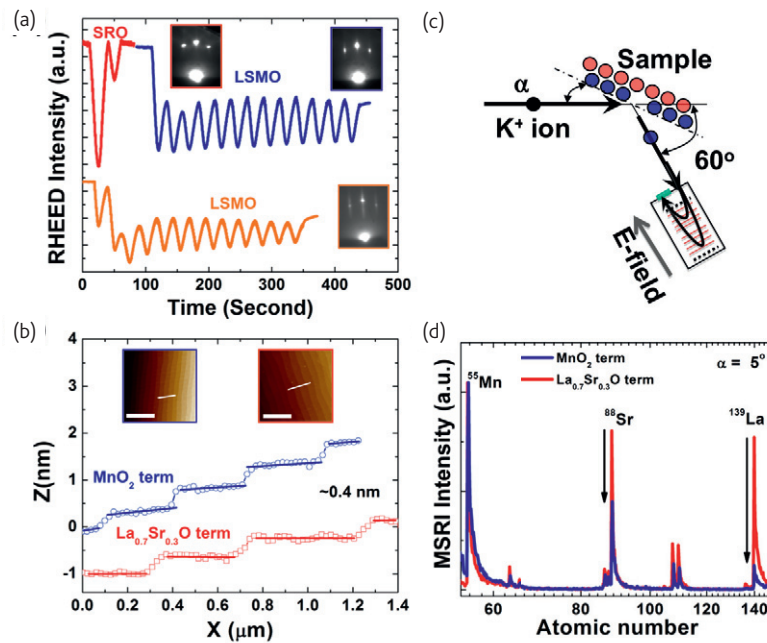


Fig. 3 Epitaxial design of BFO/LSMO heterointerfaces. (a) RHEED pattern and the specular intensity monitored during the growth. (b) Topography of LSMO thin films with nominal  $\text{La}_{0.7}\text{Sr}_{0.3}\text{O}$  and  $\text{MnO}_2$  terminations. The insets show the atomic force microscopy images used to obtain the line profiles. (c) Schematic of the time-of-flight ion scattering and recoiled ion spectroscopy experiment setup. (d) Mass spectroscopy of recoiled ions (MSRI) spectra of LSMO thin films with nominal  $\text{MnO}_2$  and  $\text{La}_{0.7}\text{Sr}_{0.3}\text{O}$  terminations. Reproduced from<sup>29</sup> with permission from National Academy of Sciences.

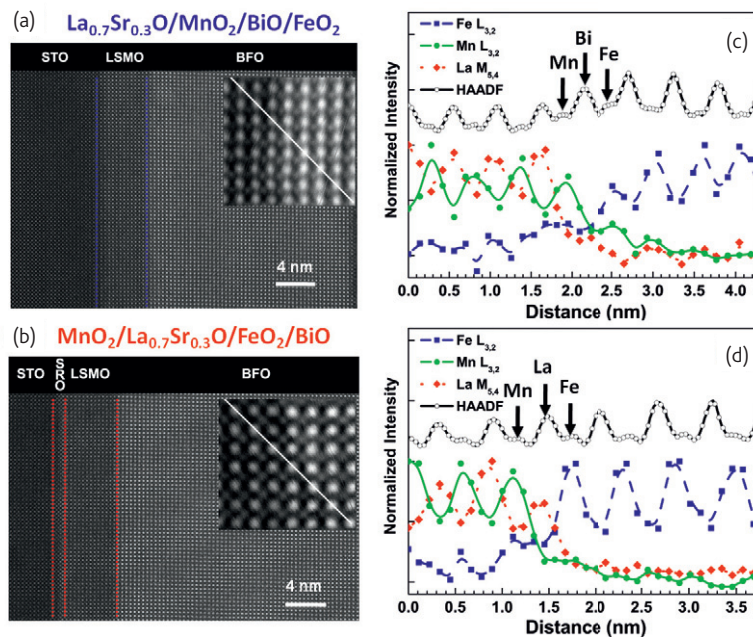


Fig. 4 Layer architectures of designed BFO/LSMO heterointerfaces. STEM images of the samples with both (a)  $\text{MnO}_2$ -terminated ( $\text{La}_{0.7}\text{Sr}_{0.3}\text{O}-\text{MnO}_2-\text{BiO}-\text{FeO}_2$ ) and (b)  $\text{La}_{0.7}\text{Sr}_{0.3}\text{O}$ -terminated ( $\text{MnO}_2-\text{La}_{0.7}\text{Sr}_{0.3}\text{O}-\text{FeO}_2-\text{BiO}$ ) interfaces. (c, d) Integrated EELS signals of the Fe  $L_{3,2}$ , Mn  $L_{3,2}$  and La  $M_{5,4}$  absorption edges for (c)  $\text{MnO}_2$ -terminated and (d)  $\text{La}_{0.7}\text{Sr}_{0.3}\text{O}$ -terminated interfaces. The data were simultaneously recorded along the lines displayed in the corresponding STEM images (insets of Figs. a,b). The arrows label the atoms positions across the interfaces. Reproduced from<sup>29</sup> with permission from National Academy of Sciences.



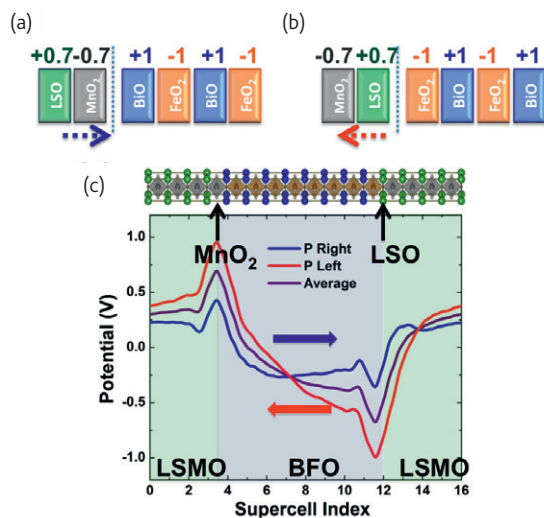


Fig. 5 Electronic reconstruction across BFO/LSMO heterointerfaces. Schematics of atomic stacking sequences across  $\text{La}_{0.7}\text{Sr}_{0.3}\text{O}-\text{MnO}_2-\text{BiO}-\text{FeO}_2$  (a) and  $\text{MnO}_2-\text{La}_{0.7}\text{Sr}_{0.3}\text{O}-\text{FeO}_2-\text{BiO}$  (b) interfaces. (c) First-principles calculations of electronic reconstruction across BFO/LSMO heterointerfaces. The two interfacial atomic planes between the  $\text{FeO}_2$  and  $\text{MnO}_2$  planes were chosen to be asymmetric, i.e. one interface is BiO and the other interface is  $\text{La}_{0.5}\text{Sr}_{0.5}\text{O}$ . The ferroelectric polarization directions (solid arrows) tend to be parallel to the directions of interface dipoles (dashed arrows). Reproduced from<sup>29</sup> with permission from National Academy of Sciences.

to quantitatively estimate the fraction of the surface that is occupied by a particular chemical species. How does this desorption process occur at the surface? Does this happen at exactly a monolayer scale? These are questions that would significantly enhance our ability to create uniformly terminated surfaces of arbitrary chemical nature.

To shed light on the atomic structure of the heterointerfaces, scanning transmission electron microscopy (STEM) and atomic-scale electron energy-loss spectroscopy (EELS) analysis are invaluable<sup>33</sup>. For both heterostructures, the cross-section STEM images (Figs. 4a and b) suggest atomically abrupt and highly controlled epitaxial interfaces between the LSMO and the BFO layers. The characteristics of the Fe, Mn, and the La EELS signals (Figs. 4c and d) reflect the expected atomic structure within the LSMO and the BFO layers and the modulations of the individual EELS signals at the interface suggest sharp chemical profiles in the interface plane. Thus, the heterointerfaces between BFO and LSMO can be engineered to exhibit two different terminations, providing an ideal platform to investigate novel coupling phenomena.

### Charge reconstruction and its influence on bulk ferroelectric polarization

With such engineered heterointerfaces, one can proceed to examine how the different interfacial structures impact the nature of the electronic interactions at these heterointerfaces. When materials with very different electronic properties are brought together, two key factors, work function difference and valence mismatch must be taken into account. The former leads to a variety of intriguing phenomena and forms the cornerstone of the semiconductor industry. The latter is one of the focal points of

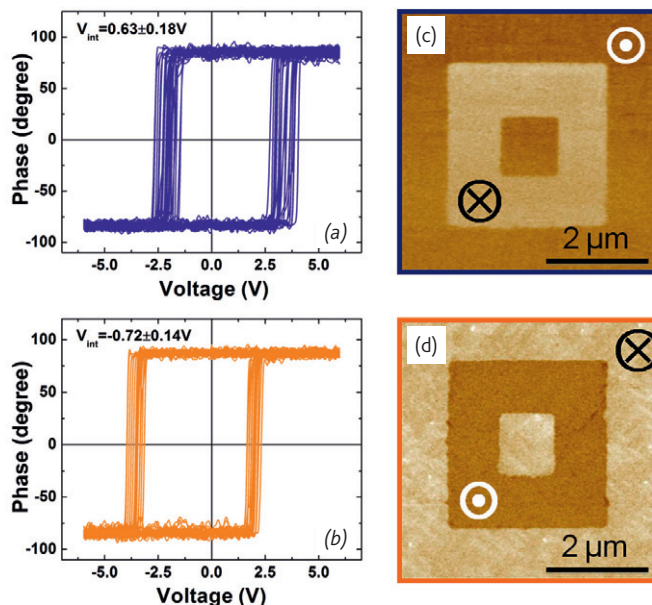


Fig. 6 Interface controls of ferroelectric polarization states. Typical quasistatic piezoresponse hysteresis loops with (a)  $\text{La}_{0.7}\text{Sr}_{0.3}\text{O}-\text{MnO}_2-\text{BiO}-\text{FeO}_2$  and (b)  $\text{MnO}_2-\text{La}_{0.7}\text{Sr}_{0.3}\text{O}-\text{FeO}_2-\text{BiO}$  interfaces. The samples used in the study are 150 nm BFO thin films with 5 nm LSMO bottom electrodes, and 100 nm Au top electrodes. (c, d) Out-of-plane PFM images of as-grown BFO/LSMO heterostructures with (c)  $\text{La}_{0.7}\text{Sr}_{0.3}\text{O}-\text{MnO}_2-\text{BiO}-\text{FeO}_2$  and (d)  $\text{MnO}_2-\text{La}_{0.7}\text{Sr}_{0.3}\text{O}-\text{FeO}_2-\text{BiO}$  interfaces. The dark (bright) contrast is correlated with the upward (downward) ferroelectric polarization. Reproduced from<sup>29</sup> with permission from National Academy of Sciences.

recent studies on oxide interfaces, and leads to the emergence of a nontrivial two-dimensional electron system<sup>13, 15, 16</sup> through the so-called polar discontinuity (valence mismatch) mechanism<sup>34</sup> in the model heterostructures of  $\text{LaAlO}_3$  and STO (Fig. 2a).

A similar valence mismatch is also present in the current BFO/LSMO system as shown in Fig. 5a and Fig. 5b. Using the nominal bulk valences for both the LSMO and BFO layers, the sheet charge density at the  $\text{MnO}_2$ -terminated interface (Fig. 5a) can be described as  $+0.7e/-0.7e/+1e/-1e$ . This results in a nominal positive charge of  $+0.15e$  at the interface<sup>35</sup>. Since the LSMO layer is metallic, the interface polar discontinuity or valence mismatch is mainly screened through the Thomas-Fermi screening in the LSMO layer. Thus the spatial separation between the interface charge and screening charge will lead to an interface dipole at the interface. Similarly, the opposite interface dipole is formed at the  $\text{La}_{0.7}\text{Sr}_{0.3}\text{O}$ -terminated interface (Fig. 5b). This interface dipole can develop into an electrostatic potential barrier across the interface, and further influence the polarization states in the ferroelectric layer.

This interface electronic reconstruction can be further understood through first-principles theoretical calculations. Fig. 5c shows atomic-scale electrostatic potential profiles across the two inequivalent interfaces with two possible ferroelectric polarization configurations. We note that the contribution of the ferroelectric polarization switches sign as the polarization is reversed; therefore the intrinsic electrostatic potential difference resulting from the interface valence mismatch can be estimated through the average of the electrostatic potentials for two opposite polarizations (purple curve in Fig. 5c), in which a potential step of  $\sim 1.3$  V forms between the two asymmetric interfaces.

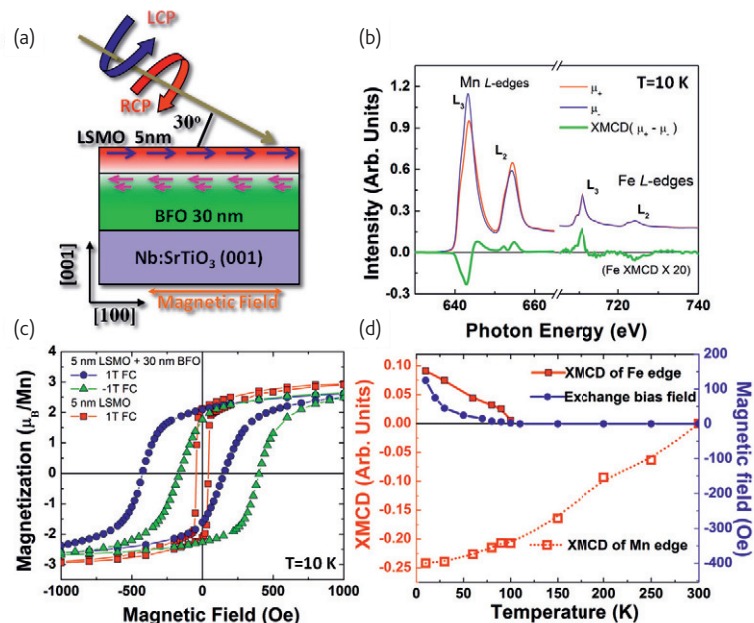


Fig. 7 Emergence of novel interface magnetic state at LSMO/BFO heterointerfaces. (a) Schematic of experimental setup and interface spin configurations. The arrows indicate the spin orientations. (b) Novel interfacial magnetic state at LSMO/BFO heterointerface revealed with x-ray magnetic circular dichroism measurements. (c) Magnetic hysteresis loops of LSMO/BFO heterostructure measured at 10 K after 1 T field cooling (FC) along the [100] direction. (d) Temperature dependence of interfacial magnetic states as well as the exchange bias coupling. Reproduced from<sup>27</sup> with permission from American Physical Society.

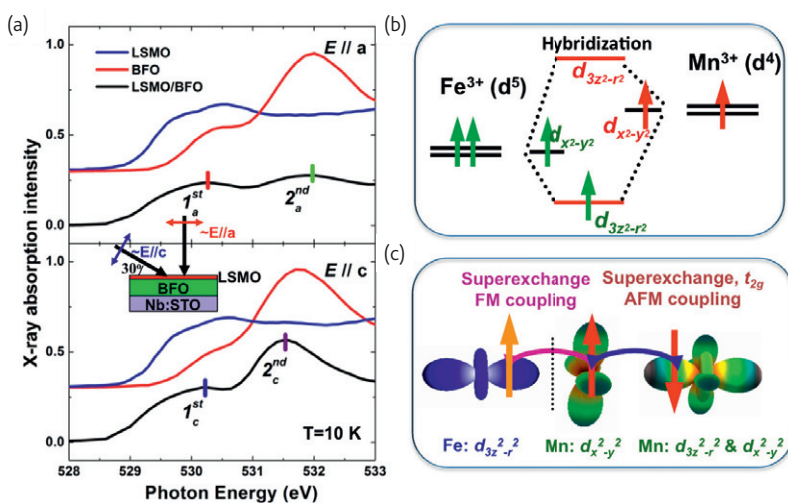


Fig. 8 Orbital reconstruction at LSMO/BFO heterointerfaces. (a) Linearly polarized oxygen K-edge XAS spectra with polarization direction in-plane (top panel) and out-of-plane (bottom panel). (b) Schematic of interface electronic orbital reconstruction through the interfacial hybridization. The arrows represent the spins orientations of the d electrons. (c) Proposed interface spin configuration and coupling mechanism with  $d_{x^2-y^2}$  orbital ordering at the interfacial LSMO layer. The arrows represent the spins orientations in the transition metals. Reproduced from<sup>27</sup> with permission from American Physical Society.

Experimentally, in the current system the magnitude of the interface-induced electrostatic potential barrier can be estimated quantitatively from physical measurements, such as the piezoresponse hysteresis loops (Figs. 6a and b). In such measurements, because of the difference between the work functions of the bottom and the top electrodes, the hysteresis loops are typically asymmetric with a biased-voltage

of  $V_{\text{int}} = (V_+ + V_-)/2$ , where  $V_+$  ( $V_-$ ) is the positive (negative) coercive voltage<sup>36</sup>. As these data show, the biased-voltages were determined to be  $0.63 \pm 0.18$  and  $-0.72 \pm 0.14$  V for the heterostructure with  $\text{MnO}_2$ - and  $\text{La}_{0.7}\text{Sr}_{0.3}\text{O}$ -terminated interfaces, respectively. Thus the interface induced electrostatic potential barrier can be estimated as the difference between the biased-voltages ( $\sim 1.35$  V), consistent with the result

obtained by first-principles calculations<sup>29</sup>. Furthermore, the as-grown polarization direction is directly correlated with the interface termination of the heterostructure through the coupling with the interface induced electrostatic potentials. For samples with a different interface atomic stacking sequence, the ferroelectric polarization directions are different, with upward and downward polarization states for MnO<sub>2</sub>-terminated (Fig. 6c) and La<sub>0.7</sub>Sr<sub>0.3</sub>O-terminated, respectively.

We note that as the thickness of the BFO layer is decreased down to a few nm, the internal field due to the interface dipole is significantly enhanced and interacts strongly with the ferroelectric order of the BFO layer. Thus, an interesting question emerges, namely, what happens to the stability of the polar state as the thickness is progressively reduced? Can the ferroelectric state be destabilized, leading to the stabilization of, perhaps a nonpolar or antipolar state? If yes, to what thickness does this propagate? High-resolution transmission electron microscopy provides a direct tool for such studies, in which one can probe the ferroelectric polarization profile across the interface<sup>37</sup> with atomic resolution, as well as its correlation with the presence of interface charges and dipoles<sup>38</sup>, and even study how the interface polar states can interact with the ferroelectric polarization switching dynamics<sup>39,40</sup>. Nevertheless, it would also be of great interest and fundamental importance to further explore the influence of the interface engineering to the functionalities of the ferroelectric devices, since they are strongly coupled with the interface electronic structures.

Similarly, in the system of LSMO/STO interfaces, theoretical calculations and experimental studies reveal the presence of an electrostatic potential barrier across the interface due to the valence mismatch<sup>41,42,35</sup>. The results from these two systems together with the seminal work of LaAlO<sub>3</sub> and SrTiO<sub>3</sub> interfaces strongly suggest that besides the work function difference (or band bending), valence mismatch is another fundamentally important factor influencing interface electronic reconstruction. A direct probe of the band structure and band alignment across the interface would provide strong evidence for the electronic reconstruction, which can be achieved through the use of atomically resolved cross-sectional scanning tunneling microscopy<sup>43</sup> or/and transmission electron microscopy. We also note that this interfacial electronic reconstruction can further interact with the spin and orbital degrees of freedom across the interface and provide a novel pathway to engineer the interfacial magnetic states<sup>12,44</sup>.

## Orbital reconstruction and interface magnetism

In addition to the electronic reconstruction discussed in the previous section, spin and orbital reconstructions can also occur at the interface. When two materials with different spin structures are brought together with atomic precision, the spin frustration across the interface can lead to novel interfacial spin states (Fig. 2b)<sup>14,27</sup>. Moreover, the orbital degree of freedom can play an important role in modulating the magnetic coupling across the heterointerfaces (Fig. 2c)<sup>17,27</sup>. In the current system, BFO shows a G-type antiferromagnetic spin structure; while the LSMO layer is ferromagnetic. Thus no matter what the coupling mechanism is involved across the interface, such a spin configuration at the interface is energetically unfavorable. The competition between the interface

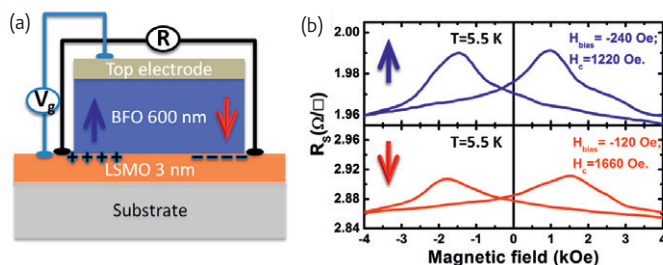


Fig. 9 Magnetoelectric coupling across BFO/LSMO heterointerfaces. (a) Schematics of a ferroelectric field-effect transistor built with BFO and LSMO layers. The arrows indicate the out-of-plane ferroelectric polarization directions. (b) Representative magnetotransport measurements carried out with upward (top panel) and downward (bottom panel) ferroelectric polarizations after the gate-voltage switching. Reproduced from<sup>28</sup> with permission from Nature publishing group.

coupling and the different ground states of bulk BFO and LSMO leads to spin frustration and thus a novel spin state at the interface<sup>27</sup>.

One of the most effective techniques to investigate the interface spin state is x-ray magnetic circular dichroism (XMCD) in the total electron yield mode<sup>45,46</sup> which is both surface sensitive and element specific. Using the LSMO/BFO heterostructure shown in Fig. 7a, one can directly probe the interface spin structure of BFO layer. Fig. 7b shows the XMCD spectra for both Mn- and Fe- *L* edges at 10 K. The dichroism of Mn is consistent with the previous measured values<sup>47</sup>; while a dramatically large XMCD is unexpectedly observed in the Fe *L*-edge<sup>48</sup>. This data strongly suggests that in the top few atomic layers of the BFO film a new magnetic spin structure is present that is markedly different from that in the remainder of the BFO film (Fig. 7a). Additionally, the opposite signs observed in Mn and Fe XMCD, suggest that the coupling between the Mn bulk and Fe interfacial spins is anti-parallel.

We note that this uncompensated interface magnetic state can further influence the magnetic properties of the LSMO layer through the so-called exchange bias coupling<sup>49,50</sup>. Magnetic measurements on LSMO/BFO heterostructures (Fig. 7c) show both a strong enhancement of the coercive field (~275 Oe) compared to that of the LSMO/STO sample (~40 Oe) and a shift of the hysteresis loop leading to an exchange bias field of 140 Oe. Temperature dependent measurements (Fig. 7d) further reveal a causal relationship between the novel interfacial magnetic state and the exchange bias coupling, with the same transition temperature of around 100 K.

To understand coupling mechanisms across interfaces, knowledge about the orbital structures at the interface is fundamentally important, since the magnetic coupling between the metal ions is mainly determined by the occupancy of *d*-orbitals<sup>51-53</sup>. One pathway to achieve this is through probing of the oxygen *K*-edge with linearly polarized x-rays<sup>27</sup>. Because of the strong bonding/coupling between oxygen anions and transition metal cations, the oxygen *K*-edge x-ray absorption spectra are strongly correlated with the type and environment of the transition oxides. Moreover, linearly polarized x-rays can naturally probe the orbital structures with different geometry occupations. For instance, in-plane (out of plane) linearly polarized x-ray is mainly sensitive to the  $d_{x^2-y^2}$  ( $d_{3z^2-r^2}$ ) orbital, as shown in Fig. 8a. Thus one can trace the origin of the spectral feature in the LSMO/BFO heterostructure by comparing with the

reference spectra of the BFO and LSMO layers. Clearly, the peak labeled as  $2^{nd}$  ( $2^{nd}$ ) corresponds to the  $d_{x^2-y^2}$  ( $d_{3z^2-r^2}$ ) orbital of the BFO layer, since LSMO does not display any peak near this energy region; while the rest ( $1^{st}$  and  $1^{st}$ ) are related to the mixture of both BFO and LSMO layers, since characteristic peaks are present for both materials around this energy region. One can also obtain information about the electronic structure across the interface by tracing the characteristic peak positions. The clear and intense red shift of the  $2^{nd}$  peak suggests that along the  $c$ -direction a hybridized state between LSMO and BFO  $d_{3z^2-r^2}$  orbitals is formed (Fig. 8a). Through the coupling, the hybridization modifies the original energy levels and breaks the degeneracy of the Mn  $d_{x^2-y^2}$  and  $d_{3z^2-r^2}$  orbitals at the interface (Fig. 8b). As suggested by the oxygen  $K$ -edge study, the BFO  $d_{3z^2-r^2}$  electrons occupy the lower energy bonding orbital, thus the Mn adopts an  $d_{x^2-y^2}$  orbital state, since this energy level is lower than that of the antibonding  $d_{3z^2-r^2}$  orbital state. As a consequence,  $d_{x^2-y^2}$  orbital ordering is favored at the interface for LSMO (Fig. 8b).

With knowledge about the orbital structure at the interface, one can attain a greater insight into the spin configuration across the interface, as shown in Fig. 8c. The superexchange coupling<sup>54-56</sup> between the  $Fe^{3+}$  and the  $d_{x^2-y^2}$  orbitally ordered  $Mn^{3+}$  as well as between the  $Fe^{3+}$  and  $Mn^{4+}$  are both expected to be ferromagnetic. Moreover, the  $d_{x^2-y^2}$  orbital ordering naturally leads to antiferromagnetic coupling between the interfacial Mn layer and its neighboring Mn layer via the superexchange interaction between neighboring  $t_{2g}$  spins. Thus, through this model, the interfacial Fe spins and the Mn spins in the bulk LSMO region are coupled antiferromagnetically as suggested by the XMCD measurement. Finally the spin frustration across the interface leads to a novel magnetic state at the BFO interfacial sublattice, as revealed by XMCD measurements<sup>27</sup>.

### Magnetoelectric coupling: electric field control magnetism

In the previous section, we have shown that at the interface between LSMO and BFO, a new magnetic state has been induced as a consequence of the overall electronic orbital reconstruction at the heterointerface, and this magnetic state can further lead to an exchange bias coupling across the heterointerface. By taking advantage of the coupling between the spin and orbital degrees of freedom, one can also find a novel pathway toward controlling the magnetism of a system using an electric field. Since the orbital degree of freedom is correlated to the  $d$  electron occupancy, in principle a change of the electronic state of the interface induced by switching the ferroelectric polarization direction can modulate the interface magnetic coupling and eventually lead to magnetoelectric coupling<sup>9</sup>. To verify this, a typical vertical ferroelectric field effect transistor device<sup>57,58</sup> (Fig. 9a) was fabricated, in which the BFO layer was used as the ferroelectric gate to modulate the charge state at the interface with the LSMO channel. For an *upward* (*downward*) ferroelectric polarization state, holes will be accumulated (depleted) at the interface through ferroelectric screening. Accordingly, the sheet resistances are distinctly different between different ferroelectric polarizations (Fig. 9b), suggesting that the electronic state of the conducting channel LSMO layer is indeed tunable through the ferroelectric polarization. To obtain direct information about the magnetic coupling in the heterostructure,

magneto-transport across the LSMO layer has been carried out (Fig. 9b), and the peak positions of the magnetoresistance curves are correlated with the coercive fields from the magnetic measurements. Thus, one can deduce both coercive and exchange bias fields through these transport measurements. For upward polarization state, the coercive and exchange-bias fields were measured to be around 1220 Oe and 240 Oe, respectively. On the other hand, very different magnetic anisotropy was obtained for the downward case, with an enhancement of coercive field (1660 Oe) and a suppression of the exchange-bias field (120 Oe). Further measurements have also shown that this effect can be reversibly controlled by isothermal switching of the ferroelectric polarization of the BFO layer<sup>28</sup>. This finding is an important step towards the electric field control of magnetism, and may enable a new class of electrically controllable spintronic devices, such as multiferroic tunnel junctions, spin valves, and possibly tunable spin polarized two-dimensional electron gases. Although in the current system the magnetoelectric coupling transition temperature is only around 100 K, higher temperatures might be achievable in similar systems through engineering/design of the interfacial magnetic coupling strength and the correlated orbital degree of freedom. From application point of view, it would be a tremendous breakthrough, if one can enhance the transition temperature above room temperature.


### Outlook and future prospects

In summary, BFO/LSMO heterostructures present an intriguing model system to study the interactions between various degrees of freedom. In addition, it has been demonstrated that the interface properties can be utilized to control the ferroelectric<sup>29</sup> and ferromagnetic<sup>28</sup> properties of the heterostructures. The results provide novel approaches to design functionalites through complex oxide interfaces.

In the past decade, although substantial progress has been achieved in understanding the properties of interfaces, several challenges still remain. The first problem is related to the coupled degrees of freedom. Among all of these degrees of freedom, the orbital degree of freedom is the least studied; however this topic has received a great deal of attention recently, mainly due to its strong correlation to exotic physical phenomena<sup>59</sup> such as superconductivity and multiferroicity. Thus, the manipulation of the orbital degree of freedom across the interface can be used as a new knob to control desirable phenomena<sup>17,19,27</sup>, leading to breakthroughs in fundamental physics and applied electronics. On the other hand, although lattice reconstruction (such as through epitaxial strain) has been extensively studied in the past, another subtle yet interesting structural interaction known as octahedral rotation, has emerged recently and drawn considerable research interest<sup>60-64</sup>. When materials with different oxygen *octahedral rotation* symmetry meet at the interface (as shown in Fig. 2d), the discontinuity of the rotation will lead to a new phase with totally different symmetry and possibly novel properties.

Another open question is related to the practical applications of such interfacial phenomena, or how to incorporate the complex oxide heterointerface onto a semiconductor chip, while not sacrificing the emergent phenomena associated with the interface. One pathway to achieve this is to use a thin perovskite layer, such as  $SrTiO_3$ , as a



buffer on top of a silicon substrate to assist the growth of perovskite oxides. Indeed, the emergence of ferroelectricity has been observed in a heterostructure of SrTiO<sub>3</sub> and silicon<sup>65</sup>; and recently a two-dimensional electron gas has also been observed at the interface between LaAlO<sub>3</sub> and SrTiO<sub>3</sub> with a silicon substrate<sup>66</sup>. Conversely, the growth of non-perovskite materials on top of perovskite substrates can also provide a broad horizon for the exploration of emergent phenomena. For example, it has been demonstrated that the perovskite substrate can serve as a great template for the growth of iron-based superconductors<sup>67</sup>; and more strikingly, it has recently been revealed that the interaction between an ultrathin (one unit cell) layer of the superconductor FeSe and an SrTiO<sub>3</sub> substrate can lead to a dramatic enhancement of the superconducting transition temperature compared with the bulk<sup>68</sup>. These pioneering works have opened new pathways for the design of novel interfacial phenomena across dissimilar structures. 

## Acknowledgments:

The authors would like to acknowledge the work of four collaborators including Robert Dynes, Stephen Wu and Shane Cybart at the University of California, Berkeley; Chi-Chang Kao and Jun-Sik Lee at SLAC National Accelerator Laboratory; Dario Arena at the Brookhaven National Laboratory; Weidong Luo, Satoshi Okamoto, Albina Borisevich, Sergei Kalinin, Sokrates Pantelides and Stephen Pennycook at Oak Ridge National Laboratory; Elke Arenholz, Andreas Scholl and Jinghua Guo at Lawrence Berkeley National Laboratory. Additionally, the authors would like to acknowledge the contributions of the current and former members at the University of California, Berkeley including James Clarkson, Qing He, Jayakanth Ravichandran, John Heron, Mikel Holcomb, Mark Huijben, Lane Martin, Marta Rossell, Guneeta Singh-Bhalla, Morgan Trassin, Chan-Ho Yang, Seung-Yeul Yang, Di Yi and Jinxing Zhang. This work was supported by Director Office of Science, Office of Basic Energy Science, Materials Science and Engineering Division of the US Department of Energy under Contract No. DE-AC02-05CH11231.

## Reference:

- Dagotto, E., *Rev Mod Phys.* (1994) **66**, 763.
- Imada, M., Fujimori, A. and Tokura, Y., *Rev Mod Phys.* (1998) **70**, 1039.
- Tokura, Y., *Colossal-Magnetoresistive Oxides*, Gordon & Breach Science Publishers, (1999).
- Salamon, M. B. and Jaime, M., *Rev Mod Phys* (2001) **73**, 583.
- Dagotto, E., *Nanoscale Phase Separation and Colossal Magnetoresistance*, Springer, (2003).
- Dawber, M., Rabe, K. M. and Scott, J. F., *Rev Mod Phys* (2005) **77**, 1083.
- Fiebig, M., *J Phys D: Appl Phys* (2005) **38**, R123.
- Cheong, S. W. and Mostovoy, M., *Nature Mater.* (2007) **6**, 13.
- Ramesh, R. and Spaldin, N. A., *Nature Mater.* (2007) **6**, 21.
- Ueda, K., Tabata, H. and Kawai, T., *Science* (1998) **280**, 1064.
- Ohtomo, A. et al., *Nature* (2002) **419**, 378.
- Yamada, H. et al., *Science* (2004) **305**, 646.
- Ohtomo, A. and Hwang, H. Y., *Nature* (2004) **427**, 423.
- Chakhalian, J. et al., *Nature Phys* (2006) **2**, 244.
- Brinkman, A. et al., *Nature Mater* (2007) **6**, 493.
- Reyren, N. et al., *Science* (2007) **317**, 1196.
- Chakhalian, J. et al., *Science* (2007) **318**, 1114.
- Smadici, S. et al., *Phys Rev Lett* (2007) **99**, 196404.
- Benckiser, E. et al., *Nature Mater* (2011) **10**, 189.
- Heber, J., *Nature* (2009) **459**, 28.
- Mannhart, J. and Schlom, D. G., *Science* (2010) **327**, 1607.
- Zobko, P. et al., *Annu Rev Condens Matter Phys* (2011) **2**, 141.
- Hwang, H. Y. et al., *Nature Mater* (2012) **11**, 103.
- Chakhalian, J., Millis, A. J. and Rondinelli, J. M., *Nature Mater* (2012) **11**, 92.
- Catalan, G. and Scott, J., *Adv Mater* (2009) **21**, 2463.
- Chu, Y. H. et al., *Materials Today* (2007) **10**, 16.
- Yu, P. et al., *Phys Rev Lett* (2010) **105**, 027201.
- Wu, S. W. et al., *Nature Mater* (2010) **9**, 756.
- Yu, P. et al., *PNAS* (2012) **109**, 9710.
- Kawasaki, M. et al., *Science* (1994) **2**, 1540.
- Rijnders, G. et al., *Appl Phys Lett* (2004) **84**, 505.
- Rabalais, J. W., *Principles and applications of ion scattering spectroscopy* (John Wiley & Sons, Inc. 2003)
- Erni, R. et al., *Phys Rev Lett* (2009) **102**, 096101.
- Nakagawa, N., Hwang, H. Y. and Muller, D. A., *Nature Mater* (2006) **5**, 204.
- Hikita, Y. et al., *Phys Rev B* (2009) **79**, 073101.
- Scott, J. F., *Ferroelectric Memories* (Springer, 2000).
- Jia, C. L. et al., *Nature Mater* (2007) **6**, 64.
- Chang, H. J. et al., *Adv Mater* (2011) **23**, 2474.
- Nelson, C. T. et al., *Science* (2011) **334**, 968.
- Chang, H. et al., *J Appl Phys* (2011) **110**, 052014.
- Burton, J. D. and Tsymal, E. Y., *Phys Rev B* (2010) **82**, 161407.
- Zheng, B. and Binggeli, N., *Phys Rev B* (2010) **82**, 245311.
- Chiu, Y. P. et al., *Adv Mater* (2011) **23**, 1530.
- Boschker, H. et al., *Adv Mater* (2012) 10.1002/adfm.201102763.
- Regan, T. J. et al., *Phys Rev B* (2001) **64**, 214422.
- Ohldag, H. et al., *Phys Rev Lett* (2001) **87**, 247201.
- Kavich, J. J. et al., *Phys Rev B* (2007) **76**, 014410.
- Bea, H. et al., *Appl Phys Lett* (2005) **87**, 072508f.
- Meiklejohn, W. H. and Bean, C. P., *Phys Rev* (1957) **105**, 904.
- Nogués, J. and Schuller, I. K., *J Magn Magn Mater* (1999) **192**, 203.
- Anderson, P. W., *Phys Rev* (1950) **79**, 350.
- Goodenough, J. B., *Phys Rev* (1955) **100**, 546.
- Kanamori, J., *J Phys Chem Solid* (1959) **10**, 87.
- Anderson, P. W., *Phys Rev* (1950) **79**, 350.
- Goodenough, J. B., *Phys Rev* (1955) **100**, 546.
- Kanamori, J., *J Phys Chem Solid* (1959) **10**, 87.
- Mathews, S. et al., *Science* (1997) **276**, 238
- Anh, C. H. et al., *Science* (1999) **284**, 1152.
- Tokura, Y. and Nagaosa, N., *Science* (2000) **288**, 462.
- Borisevich, A. et al., *Phys Rev Lett* (2010) **105**, 087204 (2010)
- He, J. et al., *Phys Rev Lett* (2010) **105**, 227203.
- Rondinelli, J. M. and Spaldin, N. A., *Phys Rev B* (2010) **82**, 113402.
- May, S. J. et al., *Phys Rev B* (2011) **83**, 153411.
- Rondinelli, J. M. and Spaldin, N. A., *Adv Mater* (2011) **23**, 3363.
- Warusawithana, M. P. et al., *Science* (2009) **324**, 367.
- Park, J. W. et al., *Nature Commun* (2010) **1**, 94.
- Lee, S. et al., *Nature Mater* (2010) **9**, 397.
- Wang, Q. Y. et al., *Chin Phys Lett* (2012) **29**, 037402.